Parametric characterization of surface plasmon polaritons at a lossy interface

Rosario Martinez-Herrero[1] **Aitor Garcia-Ruiz,**[1] **and Alejandro Manjavacas**[2,*]

[1]*Departamento de Óptica, Universidad Complutense de Madrid, 28040 Madrid, Spain*
[2]*Department of Physics and Astronomy, University of New Mexico, Albuquerque, New Mexico 87131, USA*

[*]*manjavacas@unm.edu*

Abstract: Using exact solutions of Maxwell's equations, we investigate the evolution of the transversal profile of a surface plasmon polariton (SPP) packet propagating along a planar interface between a dielectric and a lossy metal. We introduce a parameter to measure the propagation length of the SPP packet and analyze its behavior with respect to the shape of the packet and the dielectric characteristics of the interface. Furthermore, we study the polarization properties of the SPP packet and define two parameters to quantify the fraction of the irradiance contained in the *s*- and *p*-polarization components of the associated field. Our results help to advance in the understanding of the SPP optics beyond the single-mode description.

OCIS codes: (250.5403) Plasmonics; (240.6680) Surface plasmons; (260.3910) Metal optics; (140.3295) Laser beam characterization; (240.6690) Surface waves; (350.5500) Propagation.

References and links

1. R. H. Ritchie, "Plasma losses by fast electrons in thin films," Phys. Rev. **106**, 874–881 (1957).
2. J. M. Pitarke, V. M. Silkin, E. V. Chulkov, and P. M. Echenique, "Theory of surface plasmons and surface-plasmon polaritons," Rep. Prog. Phys. **70**, 1–87 (2007).
3. S. A. Maier, *Plasmonics: Fundamentals and Applications* (Springer, 2007).
4. E. Ozbay, "Plasmonics: Merging photonics and electronics at nanoscale dimensions," Science **311**, 189–193 (2006).
5. J. A. Dionne, L. A. Sweatlock, H. A. Atwater, and A. Polman, "Planar metal plasmon waveguides: frequency-dependent dispersion, propagation, localization, and loss beyond the free electron model," Phys. Rev. B **72**, 075405 (2005).
6. G. Veronis and S. Fan, "Guided subwavelength plasmonic mode supported by a slot in a thin metal film," Opt. Lett. **30**, 3359–3361 (2005).
7. S. I. Bozhevolnyi, V. S. Volkov, E. Devaux, J. Y. Laluet, and T. W. Ebbesen, "Channel plasmon subwavelength waveguide components including interferometers and ring resonators," Nature **440**, 508–511 (2006).
8. E. Moreno, S. G. Rodrigo, S. I. Bozhevolnyi, L. Martín-Moreno, and F. J. García-Vidal, "Guiding and focusing of electromagnetic fields with wedge plasmon polaritons," Phys. Rev. Lett. **100**, 023,901 (2008).
9. A. Manjavacas and F. J. García de Abajo, "Robust plasmon waveguides in strongly interacting nanowire arrays," Nano Lett. **9**, 1285–1289 (2009).
10. C. E. H. Berger, T. A. M. Beumer, and R. P. H. K. J. Greve, "Surface Plasmon Resonance Multisensing," Anal. Chem. **70**, 703–706 (1998).
11. J. Homola, S. Yee, and G. Gauglitz, "Surface-plasmon resonance sensors: review," Sens. Actua. B: Chem. **54**, 3–15 (1999).
12. M. A. Cooper, "Optical biosensors in drug discovery," Nat. Rev. Drug. Discov. **1**, 515–528 (2002).
13. A. J. Haes and R. P. V. Duyne, "A unified view of propagating and localized surface plasmon resonance biosensors," Anal. Bioanal. Chem. **379**, 920–930 (2004).
14. J. B. Pendry, "Negative refraction makes a perfect lens," Phys. Rev. Lett. **85**, 3966–3969 (2000).

#248971 Received 31 Aug 2015; revised 14 Oct 2015; accepted 15 Oct 2015; published 23 Oct 2015

15. N. Fang, H. Lee, C. Sun, and X. Zhang, "Sub-diffraction-limited optical imaging with a silver superlens," Science **308**, 534–537 (2005).
16. D. Melville and R. Blaikie, "Super-resolution imaging through a planar silver layer," Opt. Express **13**, 2127–2134 (2005).
17. F. Wei, D. Lu, H. Shen, W. Wan, J. L. Ponsetto, E. Huang, and Z. Liu, "Wide field super-resolution surface imaging through plasmonic structured illumination microscopy," Nano Lett. **14**, 4634–4639 (2014).
18. T. V. Teperik, A. Archambault, F. Marquier, and J. J. Greffet, "Huygens-Fresnel principle for surface plasmons," Opt. Express **17**(20), 17483–17490 (2009).
19. A. Archambault, T. V. Teperik, F. Marquier, and J. J. Greffet, "Surface plasmon Fourier optics," Phys. Rev. B **79**, 195414 (2009).
20. A. R. Zakharian, J. V. Moloney, and M. Mansuripur, "Surface plasmon polaritons on metallic surfaces," Opt. Express **15**, 183–197 (2006).
21. A. Norrman, T. Setälä, and A. T. Friberg, "Exact surface-plasmon polariton solutions at a lossy interface," Opt. Lett. **38**, 1119–1121 (2013).
22. A. Norrman, T. Setälä, and A. T. Friberg, "Surface-plasmon polariton solutions at a lossy slab in a symmetric surrounding," Opt. Express **22**, 4628–4648 (2014).
23. O. El Gawhary, A. J. L. Adam, and H. P. Urbach, "Nonexistence of pure *S*- and *P*-polarized surface waves at the interface between a perfect dielectric and a real metal," Phys. Rev. A **89**, 023834 (2014).
24. R. Martínez-Herrero, P. M. Mejías, and A. Carnicer, "Evanescent field of vectorial highly non-paraxial beams," Opt. Express **16**(5), 2845–2858 (2008).
25. R. Martínez-Herrero, P. M. Mejías, and G. Piquero, *Characterization of Partially Polarized Light Fields* (Springer-Verlag, 2008).
26. P. B. Johnson and R. W. Christy, "Optical constants of the noble metals," Phys. Rev. B **6**, 4370–4379 (1972).
27. R. Martínez-Herrero, P. M. Mejías, and A. Manjavacas, "Beam width of highly-focused radially-polarized fields," Opt. Express **18**, 20817–20826 (2010).

1. Introduction

Surface plasmon polaritons (SPPs) are electromagnetic modes supported by metal-dielectric interfaces that originate from the collective oscillations of the conduction electrons of the metal [1,2]. In the last years, SPPs have been a subject of extensive investigation due to their ability to guide electromagnetic signals along the interface at visible and near-infrared frequencies, while, at the same time, keeping them confined in small transversal regions [3,4]. These extraordinary properties have been exploited in different applications including photonic interconnects [5–9], ultrasensitive biosensors [10–13], or super-resolution near-field imaging [14–17], among others.

However, in spite of the incredible amount of work on this topic, not much attention has been paid to the characterization of SPP packets beyond the single-mode description. Indeed, SPPs propagating in metal-dielectric interfaces are very often described using a single two-dimensional plane wave [3, 5]. In this context, only recent works have started to analyze the propagation of SPPs beyond the single mode description, establishing, for instance, interesting connections between optics and plasmonics through the Fourier analysis of the plasmonic modes and the Huygens-Fresnel principle [18, 19]. In addition to that, attention should be paid when introducing any simplification in the underlying physical model, since this can often lead to solutions that are no longer admissible, as it has been recently pointed out [20–23].

In this work, we use exact solutions of Maxwell's equations to analyze the evolution of the transversal profile of a SSP packet that propagates along a flat interface separating a dielectric and a lossy metal. In order to do so, we define three different parameters; the first provides information about the propagation length of the SSP packet, whereas the other two serve to characterize the polarization properties of the packet by quantifying the fraction of the irradiance contained within the *s*- and *p*-polarization components of the associated field. As an illustrative example, we compute these parameters for the case of a Gaussian SPP packet. Interestingly, we find results that are appreciably different from those that would be obtained using a single-mode description. The paper is organized as follows. In the following section we introduce the theoretical framework. In Section 3, we define the propagation length of a SSP packet

#248971 Received 31 Aug 2015; revised 14 Oct 2015; accepted 15 Oct 2015; published 23 Oct 2015

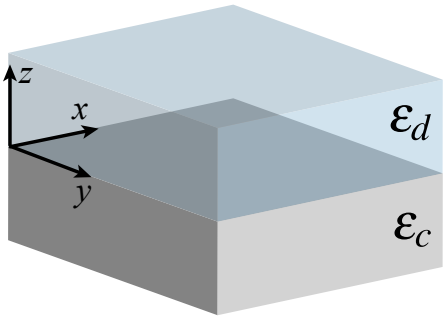

Fig. 1. Schematics of the system under study. We consider a planar interface between a dielectric and a lossy metal placed perpendicularly to the z-axis.

and we analyze its behavior with respect to the shape of the packet and the dielectric properties of the materials of the interface. Section 4 is devoted to analyze the polarization characteristics of the SPP packet. Finally, the main conclusions are summarized in Section 5.

2. Theoretical framework

We start considering an electromagnetic wave of frequency ω propagating at a planar interface between two homogeneous, nonmagnetic media, placed perpendicularly to the z-axis as shown in Fig. 1. The region $z<0$ corresponds to a metallic material and therefore is characterized by a complex dielectric function ε_c with $\mathrm{Re}\{\varepsilon_c\}<0$ and $\mathrm{Im}\{\varepsilon_c\}>0$, whereas in the half-space $z>0$ the dielectric function ε_d is real and positive. The two dielectric functions satisfy $\varepsilon_d+\mathrm{Re}\{\varepsilon_c\}<0$. Furthermore, we work in a region where no sources for the field are present [23]. Under these conditions, the electric field in medium $j=d,c$ can be written as

$$\mathbf{E}(\mathbf{r},u)=\mathbf{E}_{0,j}(u)\,e^{i\mathbf{r}\cdot\mathbf{k}_j(u)},$$

where $\mathbf{r}=(x,y,z)$ is the position, $\mathbf{k}_j=(k_{jx},k_{jy},k_{jz})$ is the wave vector, and u is a real variable. We seek rigorous surface-bound solutions of Maxwell's equations representing wave fields that decay away from the interface on both sides. Taken into account the corresponding boundary conditions, it can be shown that the components of the wave vector and the electric field in both media are given by

$$\mathbf{k}_j(u)=\left(k_x(u),\sqrt{\mathrm{Re}\left\{k_{\mathrm{sp}}^2\right\}}u,k_{jz}\right),$$

and

$$\mathbf{E}_{0j}(u)=\left(\frac{k_x(u)}{k_{\mathrm{sp}}},\frac{\sqrt{\mathrm{Re}\left\{k_{\mathrm{sp}}^2\right\}}u}{k_{\mathrm{sp}}},-\frac{k_{\mathrm{sp}}}{k_{jz}}\right),$$

respectively. In these expressions, k_{sp} is the SPP wave number, which is defined as $k_{\mathrm{sp}}^2=(\omega/c)^2\,\varepsilon_c\varepsilon_d/(\varepsilon_c+\varepsilon_d)$, while $k_{dz}^2=k_{\mathrm{sp}}^2\varepsilon_d/\varepsilon_c$ and $k_{cz}^2=k_{\mathrm{sp}}^2\varepsilon_c/\varepsilon_d$ are the wave vector components along the z-axis in the dielectric and the metal, respectively [21–23]. As discussed in the Appendix, this is not the most general expression for the wave vector of a SPP. However, it corresponds to the SPP propagating along the x-axis with the smallest attenuation in the propagation plane (xy-plane, see Fig. 1). Using these expressions, the x-component satisfies

#248971 Received 31 Aug 2015; revised 14 Oct 2015; accepted 15 Oct 2015; published 23 Oct 2015

$k_x^2(u) = k_{sp}^2 - \mathrm{Re}\left\{k_{sp}^2\right\} u^2$. When $u = 0$ we recover the well-known single-mode solution [3,21]. In a general case, these exact solutions represent inhomogeneous waves in both media, and therefore it is not possible to have a pure surface wave at the interface between a real metal and a dielectric. Nevertheless, as is pointed out in references [20–23], the square modulus of the electric field decays exponentially along the z-axis in both media. The penetration distance, d_j is independent of u and reads $d_j = 1/\mathrm{Im}\left\{k_{jz}\right\}$ [21–23]. In a similar way, the propagation length, x_0, of the SSP along the interface is determined by $\mathrm{Im}\{k_x(u)\}$ and reads $x_0 = 1/\left(2\mathrm{Im}\{k_x(u)\}\right)$.

As it is the case for free-propagating photons, a description based on a single SPP mode constitutes a first approximation to a real situation. In most of the experimentally relevant cases, SPP are generated in packets. Focusing on the field at the interface $\mathbf{E}(x,y,0) = \mathbf{E}_{sp}(x,y)$, we can construct a SSP packet as follows

$$\mathbf{E}_{sp}(x,y) = \int_{-\infty}^{\infty} du F(u) \mathbf{E}_{0j}(u)\, e^{ixk_x(u)} e^{iy\sqrt{\mathrm{Re}\left\{k_{sp}^2\right\}}u}, \tag{1}$$

where $F(u)$ is an arbitrary square integrable function and, for simplicity, we assume $x \geq 0$. From the expression above we infer that the shape of $F(u)$ plays a crucial role in the behavior and the polarization properties of the SSP packet. Taking into account the definition of $k_x(u)$, the SSP packet given in Eq. (1) can be understood as a superposition of inhomogeneous two-dimensional waves that decay at different rates along de x-axis. In this sense Eq. (1) is analogous to the evanescent component of the angular plane-wave spectrum formalism of optical fields [24, 25]. As an example of a SPP packet, in Fig. 2 we plot the squared modulus of $\mathbf{E}_{sp}(x,y)$ for a silver-vacuum interface when $F(u)$ corresponds to a Gaussian function

$$F(u) = \frac{e^{-(u/a)^2}}{a\sqrt{\pi}}, \tag{2}$$

where a is the parameter that controls the width of $F(u)$. The upper panel of Fig. 2 stands for the case with $a = 0.05$, the middle one corresponds to $a = 0.1$, and the lower one to $a = 0.1$. In all cases we assume a vacuum wavelength $\lambda = 633\,\mathrm{nm}$, which results in a dielectric function for silver $\varepsilon_c = -18.36 + i0.48$ [26]. As a increases, more components are added to the SPP packet, which results in a less collimated packet that diverges faster.

3. Propagation length of SPP packets

In this section we focus on analyzing the propagation length of a SSP packet. In order to do so, we generalize the aforementioned propagation length of a single-mode SSP to a packet by defining the parameter $\bar{x}_0$ as follows

$$\bar{x}_0 = \frac{\int_0^{\infty} dx I_{sp}(x)\, x}{\int_0^{\infty} dx I_{sp}(x)},$$

where $I_{sp}(x) = \int_{-\infty}^{\infty} dy \left|\mathbf{E}_{sp}(x,y)\right|^2$. From a physical point of view $\bar{x}_0$ determines the interval, $(0, 4\bar{x}_0)$, in which more than 75% of $\left|\mathbf{E}_{sp}(x,y)\right|^2$ is confined [25,27]. Taking into account Eq. (1) and Parseval's identity, we can rewrite the propagation length $\bar{x}_0$ as

$$\bar{x}_0 = \frac{\int_{-\infty}^{\infty} du \left|\mathbf{E}_{0d}(u) F(u)\right|^2 / \mathrm{Im}^2\{k_x(u)\}}{2\int_{-\infty}^{\infty} du \left|\mathbf{E}_{0d}(u) F(u)\right|^2 / \mathrm{Im}\{k_x(u)\}}. \tag{3}$$

It is clear from the this expression that the value of $\bar{x}_0$ is determined by the dielectric properties of the interface and by the shape of $F(u)$. Interestingly, the rate $\bar{x}_0/d_d$ can be used as a figure

#248971 Received 31 Aug 2015; revised 14 Oct 2015; accepted 15 Oct 2015; published 23 Oct 2015

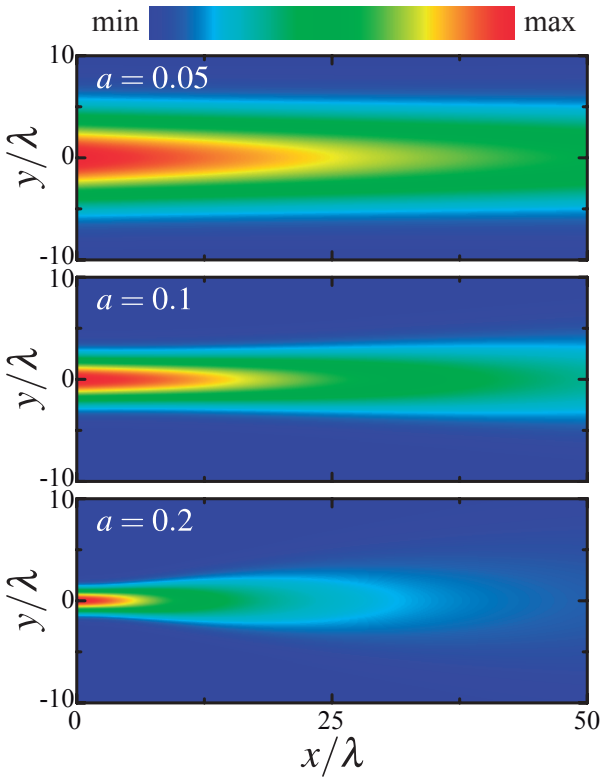

Fig. 2. Square modulus of the SPP packet field, $\mathbf{E}_{\rm sp}(x,y)$ for a silver-vacuum interface. We assume a Gaussian packet, *i.e.* $F(u)$ given by Eq. (2), with three different values of a: 0.05 (upper panel), 0.1 (middle panel), and 0.2 (lower panel). In all cases we choose a vacuum wavelength $\lambda = 633\,\text{nm}$.

of merit describing the confinement and propagation properties of SSP packet, similarly to the figure of merit introduced in [9].

When $F(u)$ is peaked around $u=0$ (*i.e.* in the paraxial limit) we can expand the integrands of Eq. (3) up to second order in u and obtain a more handy expression for the propagation length, namely

$$\bar{x}_0 = \frac{1}{2\text{Im}\left\{k_{\rm sp}\right\}} \frac{1-\frac{\langle u^2\rangle_0 \text{Re}\left\{k_{\rm sp}^2\right\}}{(1+\gamma)\left|k_{\rm sp}^2\right|}\left(\gamma+\frac{\text{Re}\left\{k_{\rm sp}^2\right\}}{\left|k_{\rm sp}^2\right|}\right)}{1-\frac{\langle u^2\rangle_0 \text{Re}\left\{k_{\rm sp}^2\right\}}{(1+\gamma)\left|k_{\rm sp}^2\right|}\left(\frac{\gamma-1}{2}+\frac{\text{Re}\left\{k_{\rm sp}^2\right\}}{\left|k_{\rm sp}^2\right|}\right)}, \tag{4}$$

where

$$\langle u^2\rangle_0 = \frac{\int_{-\infty}^{\infty} du\,|F(u)|^2\,u^2}{\int_{-\infty}^{\infty} du\,|F(u)|^2},$$

and $\gamma = |\varepsilon_c|/\varepsilon_d$. Examining Eq. (4), we observe that, for a given interface, the propagation length of a paraxial SPP packet corresponds to the propagation length of a single-mode SPP modulated by a function that decreases when parameter $\langle u^2\rangle_0$ increases. Since this parameter

#248971 Received 31 Aug 2015; revised 14 Oct 2015; accepted 15 Oct 2015; published 23 Oct 2015

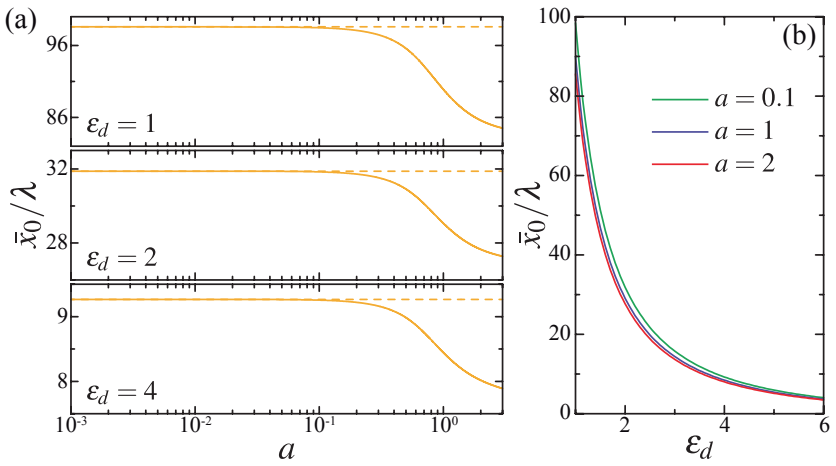

Fig. 3. Propagation length, $\bar{x}_0$, for a Gaussian SPP packet (see Eq. (2)) propagating along an interface between silver and a dielectric medium with dielectric function ε_d. Panel (a) shows $\bar{x}_0$ plotted as a function of a (solid curves) for three different values of ε_d : 1 (upper panel), 2 (middle panel), and 4 (lower panel). The dashed lines in these plots represent the propagation length for a single-mode SPP, $x_0 = 1/\left(2\mathrm{Im}\left\{k_{\mathrm{sp}}\right\}\right)$. Panel (b) shows $\bar{x}_0$ plotted as a function of ε_d for three different values of a: 0.1 (green curve), 1 (blue curve), and 2 (red curve). In all cases the vacuum wavelength λ is 633 nm.

can be understood as a measure of the width of $F(u)$, we conclude that broad SPP packets are associated with smaller propagation lengths. This result is illustrated in Fig. 3(a), where we plot $\bar{x}_0$ normalized to the vacuum wavelength $\lambda = 633$ nm for a Gaussian SSP packet (see Eq. (2)) as a function of a (solid curves). Notice that for a Gaussian SPP packet $\langle u^2 \rangle_0 = a^2/4$. We consider a silver-dielectric interface with three different values of ε_d: 1 (upper panel), 2 (middle panel), and 4 (lower panel). Comparing the propagation length of the SPP packet with that of a single-mode SPP, $x_0 = 1/\left(2\mathrm{Im}\left\{k_{\mathrm{sp}}\right\}\right)$, which is plotted in Fig. 3(a) using dashed lines, we notice that $\bar{x}_0$ can take appreciably smaller values than x_0 for large values of a. The reason is that SPP packets with larger values of a contain a larger set of wave vectors. This means that they are more localized spatially but also that they are more affected by diffraction, which leads to shorter propagation lengths. On the other hand, Fig. 3(b) shows $\bar{x}_0$ as a function of ε_d. In this case, we study three different Gaussian SSP packets with $a = 0.1$ (green curve), $a = 1$ (blue curve), and $a = 2$ (red curve). From the results shown in this figure, it is evident that the propagation length decreases when ε_d increases. The reason for this behavior is associated with the larger penetration of the field into the metal due to the reduction on the contrast between the dielectric functions of the metal and the dielectric material. This increases the Ohmic losses, thus resulting in a smaller propagation length. Similar results are obtained for other values of the Gaussian packet width a.

4. Parametric characterization of the polarization properties

The polarization properties of a SPP packet are not trivial. Indeed, analyzing Eq. (1) we observe that each mode involved in the superposition has a well defined polarization, and therefore the polarization of the entire SSP packet depends on the shape of $F(u)$. For the particular case $F(u) = \delta(u)$ we recover the well-known p-polarized single-mode SPP [3]. However, in a general case we have a nonuniform polarized field. In order to characterize the polarization properties of a SSP packet, we introduce the parameters $\rho_p(x,y)$ and $\rho_s(x,y)$, which represent

#248971 Received 31 Aug 2015; revised 14 Oct 2015; accepted 15 Oct 2015; published 23 Oct 2015

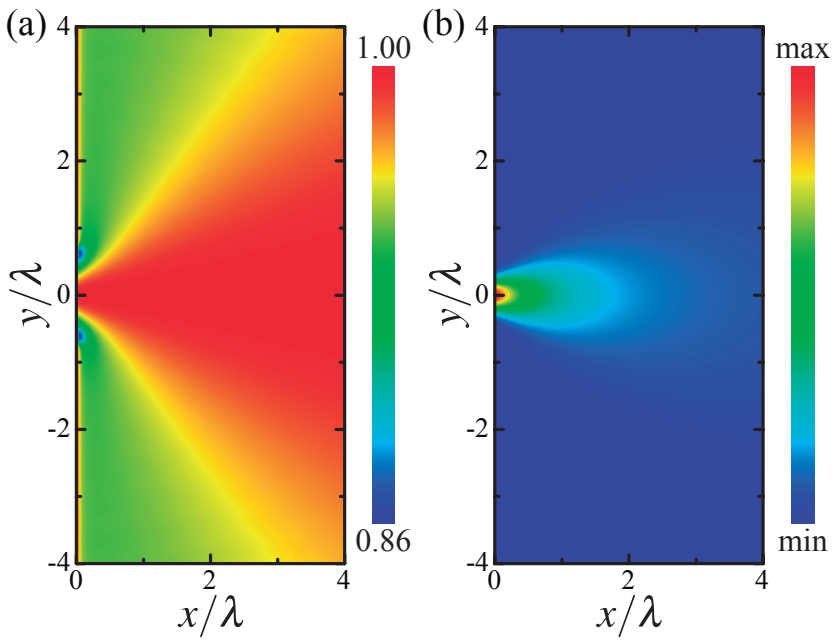

Fig. 4. Fraction of the irradiance contained in the p-component of the field of a Gaussian SPP packet, $\rho_p(x,y)$, with $a=1$ propagating on a silver-vacuum interface. (b) Square modulus of the field for the packet of panel (a). In both cases the vacuum wavelength is $\lambda = 633\,\text{nm}$.

the percentage of local irradiance associated to the p- and the s-polarization components at each point of the interface. These parameters are defined as

$$\rho_\sigma(x,y) = \frac{\left|\mathbf{E}_{\text{sp},\sigma}(x,y)\right|^2}{\left|\mathbf{E}_{\text{sp}}(x,y)\right|^2}, \tag{5}$$

where $\sigma = p,s$, and $\mathbf{E}_{\text{sp},\sigma}(x,y)$ refer to the σ-polarization component of the SSP packet field. It should be noted that we define the p and s-polarization components with respect to the xz-plane (see Fig. 1), in analogy with the case of the single-mode SPP. As expected, both $\rho_p(x,y)$ and $\rho_s(x,y)$ range from 0 to 1 and satisfy the relation $\rho_p(x,y)+\rho_s(x,y)=1$. Thus, in practice, it is only necessary to study one of them.

We explore the behavior of $\rho_p(x,y)$ in Fig. 4(a) for the case of silver-vacuum interface with $F(u)$ given in Eq. (2), $a=1$, and a vacuum wavelength of 633 nm. For our choice of parameters, the irradiance of the SPP packet is mainly concentrated in the p-component. However, comparing this figure with Fig. 4(b), where the square modulus of the analyzed SPP packet field is plotted, we notice that $\rho_p(x,y)$ only quantifies the local p-polarization content and, therefore, it does not contain any information of the irradiance. This puts in evidence the necessity of a global evaluation of the p- and s-polarization content of a SSP packet, which can be achieved by averaging the expression given in Eq. (5) along the y-axis using the SPP packet irradiance. To this end, we define the global parameters $\tilde{\rho}_p(x)$ and $\tilde{\rho}_s(x)$ as follows

$$\tilde{\rho}_\sigma(x) = \frac{\int_{-\infty}^{\infty} dy\, \rho_\sigma(x,y)\left|\mathbf{E}_{\text{sp}}(x,y)\right|^2}{\int_{-\infty}^{\infty} dy\left|\mathbf{E}_{\text{sp}}(x,y)\right|^2}, \tag{6}$$

#248971 Received 31 Aug 2015; revised 14 Oct 2015; accepted 15 Oct 2015; published 23 Oct 2015

with $\sigma = p, s$. Again, these parameters range from 0 to 1, and satisfy the relation $\tilde{\rho}_p(x) + \tilde{\rho}_s(x) = 1$. They allow us to analyze the evolution of the polarization of the SPP packet as it propagates along the interface. If we restrict ourselves to functions $F(u)$ very peaked around $u = 0$ (*i.e.* in the paraxial limit), we can approximate the right term of Eq. (6) and obtain a simpler expression for $\tilde{\rho}_p(x)$, namely

$$\tilde{\rho}_p(x) = 1 - \frac{\mathrm{Re}\left\{k_{\mathrm{sp}}^2\right\} \langle u^2 \rangle(x)}{\left|k_{\mathrm{sp}}^2\right| (1+\gamma) + \frac{2\mathrm{Re}\left\{k_{\mathrm{sp}}^2\right\} \langle u^2 \rangle(x) \mathrm{Im}^2\left\{k_{\mathrm{sp}}\right\}}{\left|k_{\mathrm{sp}}^2\right|}}, \tag{7}$$

where

$$\langle u^2 \rangle(x) = \frac{\int_{-\infty}^{\infty} du\, |F(u)|^2\, u^2 \exp\left[-\frac{x u^2 \mathrm{Re}\left\{k_{\mathrm{sp}}^2\right\} \mathrm{Im}\left\{k_{\mathrm{sp}}\right\}}{\left|k_{\mathrm{sp}}^2\right|}\right]}{\int_{-\infty}^{\infty} du\, |F(u)|^2 \exp\left[-\frac{x u^2 \mathrm{Re}\left\{k_{\mathrm{sp}}^2\right\} \mathrm{Im}\left\{k_{\mathrm{sp}}\right\}}{\left|k_{\mathrm{sp}}^2\right|}\right]}.$$

Incidentally, while a pure surface wave mode preserves its p-polarization, from Eq. (7) we conclude that the percentage of s-polarization of a SSP packet depends on the propagation length, the shape of the function $F(u)$, and the dielectric properties of the interface. Figure 5(a) shows the value of $\tilde{\rho}_p(x)$ for a Gaussian SSP packet (see Eq. (2)) propagating along a metal-dielectric interface, calculated for different values of a and ε_d, and plotted as a function of $x/\bar{x}_0$. From the results shown in this figure we observe that for $a = 0.1$ (dashed curves) the value of $\tilde{\rho}_p(x)$ is almost equal to one for the two values of ε_d, and remains constant during the analyzed propagation range. Interestingly, Gaussian SPP packets with larger values of a can present a remarkable global s-polarization content. This is the case for $a = 2$ (solid curves), for which $\tilde{\rho}_p(x)$ starts around 0.86 (0.95) for $\varepsilon_d = 4$ ($\varepsilon_d = 1$), and increases as the packet propagates, eventually reaching a constant value closer to 1. On the other hand, in Fig. 5(b) we plot $\tilde{\rho}_p(x)$ as a function of the ratio between the dielectric functions of the dielectric medium and silver, $\varepsilon_d / |\mathrm{Re}\{\varepsilon_c\}|$. We consider two different positions: $x = 0$ (green curves) and $x = 0.3\bar{x}_0$ (red curves) and two different values of a: 0.1 (dashed curves, right scale) and 2 (solid curves, left scale). We observe that, for all cases under consideration, there is a value of $\varepsilon_d / |\mathrm{Re}\{\varepsilon_c\}|$ for which $\tilde{\rho}_p(x)$ reaches a minimum. Since, k_{sp} depends on that ratio, we expect this behavior to hold for Gaussian SPP packets propagating on any planar metal-dielectric interface.

5. Conclusion

In summary, we have investigated the evolution of the transversal profile of a SPP packet propagating along a planar metal-dielectric interface. We have introduced a parameter to quantify the propagation length of the SPP packet and we have analyzed the behavior of this quantity for the case of a Gaussian SPP packet with respect to its shape and the dielectric properties of the interface. We have found that the propagation length of the packet can be appreciably smaller than that of a single-mode SPP. We have also studied the polarization properties of the SPP packet by introducing two parameters that measure the relative irradiance content associated with the p and s-components of the corresponding field. Using these parameters, we have analyzed the evolution of the polarization for Gaussian SPP packets propagating on interfaces with different dielectric properties. Interestingly, although a single-mode SPP involves only p-polarized fields, we have found that SPP packets can present a remarkable s-polarization content. Furthermore, we have found that for any Gaussian packet, there is a ratio of the dielectric functions of the materials that form the interface for which the fraction of the irradiance associated to the s-polarization component reaches a maximum value. The results presented here serve to advance

#248971 Received 31 Aug 2015; revised 14 Oct 2015; accepted 15 Oct 2015; published 23 Oct 2015

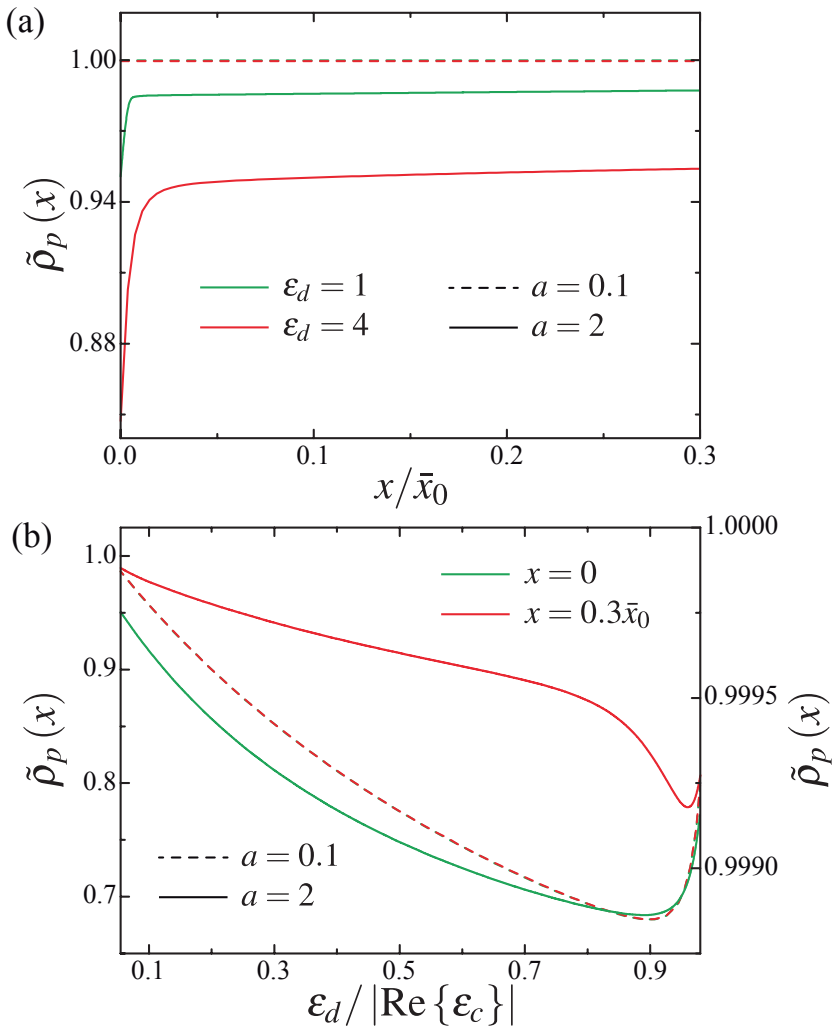

Fig. 5. Global fraction of the irradiance contained in the p-component of the field, $\tilde{\rho}_p(x)$, for a Gaussian SPP packet propagating along a metal-dielectric interface. Panel (a) shows $\tilde{\rho}_p(x)$ plotted as a function of the position x normalized to the propagation length $\bar{x}_0$. We consider two values of a: 0.1 (dashed curves), and 2 (solid curves), and two different ε_d: 1 (green curves), and 4 (red curves). Panel (b) shows $\tilde{\rho}_p(x)$ as a function of the ratio between the dielectric functions of silver and the dielectric medium, $\varepsilon_d/|\mathrm{Re}\{\varepsilon_c\}|$. We consider two different positions: $x = 0$ (green curves) and $x = 0.3\bar{x}_0$ (red curves) and two different values of a: 0.1 (dashed curves, right scale) and 2 (solid curves, left scale). In all cases the vacuum wavelength is $\lambda = 633\,\mathrm{nm}$.

#248971 Received 31 Aug 2015; revised 14 Oct 2015; accepted 15 Oct 2015; published 23 Oct 2015

in the understanding of the SPP optics beyond the single-mode description, and therefore may enable the development of new applications in plasmonics.

Acknowledgments

R.M-H. acknowledges financial support by the Ministerio de Ciencia e Innovación (Spain), under the project FIS2013-46475. A.M. acknowledges financial support from the Department of Physics and Astronomy and the College of Arts and Sciences of the University of New Mexico.

Appendix: SPP wave vector

The electric field associated with a SPP of frequency ω that propagates along a planar interface can be written as

$$\mathbf{E}_j(\mathbf{r}) = \mathbf{E}_{0j} e^{i\mathbf{r}\cdot\mathbf{k}_j},$$

where $j = d, c$ stands for the dielectric and the metal, respectively. In order to satisfy Maxwell's equations and the appropriate boundary conditions, the SPP wave vector $\mathbf{k}_j$ needs to be of the form

$$\mathbf{k}_j = (k_x, k_y, k_{jz}),$$

and fulfill the constraint

$$k_x^2 + k_y^2 = k_{\mathrm{sp}}^2.$$

Under these conditions $\mathbf{E}_{0j}$ is given by

$$\mathbf{E}_{0j} = \left(\frac{k_x}{k_{\mathrm{sp}}}, \frac{k_y}{k_{\mathrm{sp}}}, -\frac{k_{\mathrm{sp}}}{k_{jz}} \right).$$

In these expressions, $k_{\mathrm{sp}}^2 = (\omega/c)^2 \varepsilon_d \varepsilon_c / (\varepsilon_d + \varepsilon_c)$ and $k_{jz}^2 = \varepsilon_j (\omega/c)^2 - k_{\mathrm{sp}}^2$. Therefore, in the most general case we can write the SPP wave vector as

$$\begin{aligned} k_x^2 &= k_{\mathrm{sp}}^2 - u^2 \mathrm{Re}\left\{k_{\mathrm{sp}}^2\right\} - iv^2 \mathrm{Im}\left\{k_{\mathrm{sp}}^2\right\}, \\ k_y^2 &= u^2 \mathrm{Re}\left\{k_{\mathrm{sp}}^2\right\} + iv^2 \mathrm{Im}\left\{k_{\mathrm{sp}}^2\right\}, \end{aligned}$$

where u and v are real variables. In this work, we have chosen $v = 0$, which corresponds to the SPP propagating along the x-axis with the smallest attenuation in the propagation plane (xy-plane, see Fig 1).

#248971 Received 31 Aug 2015; revised 14 Oct 2015; accepted 15 Oct 2015; published 23 Oct 2015